Journal of Alloys and Compounds 526 (2012) 129–134

Contents lists available at SciVerse ScienceDirect

Journal of Alloys and Compounds

journal homepage: www.elsevier.com/locate/jallcom

Synthesis, characterization and optical properties of graphene sheets-ZnO multipod nanocomposites

Rajesh Kumar*, Rajesh Kumar Singh, Jai Singh, R.S. Tiwari, O.N. Srivastava

Nanoscience and Nanotechnology Unit, Department of Physics, Banaras Hindu University, Varanasi 221005, India

ARTICLE INFO

Article history:
Received 30 November 2011
Received in revised form 7 February 2012
Accepted 8 February 2012
Available online xxx

Keywords:
Graphene sheets
Nanocomposite
Photoluminescence spectra
Microstructures

ABSTRACT

In this paper, attention is focused on the synthesis of graphene sheets-ZnO (GSs-ZnO) multipod nanocomposite. Graphene-based composites are emerging as a new class of materials that hold promise for many curious applications in different areas. In this section, we report a suitable approach for the formation of GSs-ZnO composites through two-step processes. Initially, graphene nanosheets are synthesized by solvothermal method and in the second-stage GSs-ZnO composite is synthesized by hydrothermal method using water as solvent. It was observed that ZnO multipods were randomly dispersed on the surfaces of graphene sheets (GSs). We have also carried out the structural and optical characterizations of GSs-ZnO nanocomposites. The hybridized structure of ZnO and graphene nanosheets has been further investigated by HRTEM. The 2-D graphene nanosheets and ZnO multipod are clearly observed in the TEM microstructures indicating the formation of nanocomposite structure. Raman and FTIR investigations of GSs-ZnO nanocomposite have also shown the signature of nanocomposite formation. In addition, a photoluminescence spectrum of GSs-ZnO multipod nanocomposites displays the fluorescence quenching property.

1. Introduction

Graphene, a single atomic layer of carbon arranged in a honeycomb lattice, has attracted a lot of research interest since its discovery in 2004 [1–3]. It has been found to exhibit excellent electrical, thermal, optical, mechanical properties and room temperature Hall effect [2,4–7]. The photochemistry and photovoltaic aspects of 2-D carbon nanostructures, graphene nanosheets and graphene oxide (GO) sheets, are relatively unstudied and provide an exciting new array of ideas and applications. Although graphite and graphite oxide were known to be in existence since the last century, it has been only recently that the graphene and graphene oxide sheets have been prepared and characterized in a systematic way [8,9]. The most significant challenge in the preparation of graphene is to overcome the strong exfoliation energy of the π-stacked layers in graphite [10]. The earlier efforts to obtain graphene sheets involved the simple micromechanical cleavage of graphite, where a piece of scotch tape was used to remove individual sheets of graphene. Although the term graphene is used only for a single layer of carbon sheet, there are other related graphene structures, which have also been recently investigated. For example, graphene oxide (GO) layers have been synthesized and investigated extensively [11]. It has a characteristic peak in XRD pattern at $2\theta \approx 10–13^\circ$ (for Cu Kα wavelength) and its reduction results in the formation of graphene sheets (GSs). It should also be mentioned that few layers of graphene sheets have also been fabricated from MWCNTs, where characteristic XRD peaks of MWCNTs at 25.96° ($d_{(002)}$ = 3.43 Å) and graphene sheets at approximately 26.26° have been reported [12].

Several other methods of preparation of graphene and graphene oxide include the oxidation of graphite combined with thermal exfoliation, the treatment of graphite fluorides with alkyl lithium reagents, and the oxidation of graphite followed by strong sonication [13,14]. The factors dictating stable dispersions of graphene in various organic solvents and its interactions with substituted organic compounds have also been reported [15,16].

One obvious challenge is to utilize these 2-D carbon nanostructures as conductive carbon mats so that one can anchor semiconductor or metal nanoparticles and facilitate tailored catalytic reactions. Recently, graphene decorated with metal nanoparticles or metal oxides has also attracted a great deal of attention due to potential applications in many technological fields [17–19]. ZnO nanoparticles have recently been examined in combination with carbon nanotubes, showing an electron accepting and storing capacity of the nanotubes [20,21]. Hence, it is reasonable to expect that graphene sheets may play a similar role of providing unique 2-D architecture to support semiconductor catalyst nanoparticles. The graphene-ZnO composites might possess

* Corresponding author.
E-mail address: rajeshbhu1@gmail.com (R. Kumar).

0925-8388/$ – see front matter © 2012 Elsevier B.V. All rights reserved.
doi:10.1016/j.jallcom.2012.02.115

unusual properties as compared to their individual counterparts, and present some special features, such as high electrical and electrochemical properties, good optical transmittance, improved field emission and capacitive properties [22–25].

Solution methods are more convenient and low cost effective approach for the synthesis of oxide nanocomposites and development of different graphene-based composites [26]. ZnO, an important material in the II and VI group semiconductor, has novel applications in the optics, optoelectronics, sensors (bio, chemical and gas), UV light emitters and actuators due to its semiconducting, piezoelectric and pyroelectric properties. Furthermore, ZnO is biocompatible, which makes it suitable for biomedical applications [27]. A variety of ZnO nanostructure can be synthesized by different methods [28,29]. The growth and properties of ZnO nanostructures have been extensively studied, but there are limited reports available on ZnO-composites. Here two-step approaches have been utilized to synthesize the GSs-ZnO multipod nanocomposites. In the first step graphene sheets (GSs) have been synthesized by solvothermal method and in second step graphene sheets-ZnO (GSs-ZnO) multipod nanocomposite has been prepared employing hydrothermal method.

2. Methods

2.1. Preparation of graphene sheets (GSs)

Graphene sheets in the present work were prepared by the solvothermal method [30]. All solvothermal reactions were performed in a reactor having a maximum volume of 50 mL. A typical synthesis consists of heating a 1:1 molar ratio of sodium (2 g) and ethanol (5 ml) in a sealed reactor vessel at 220 °C for 72 h to yield a solid solvothermal product – the graphene precursor. This material is then rapidly pyrolyzed and the remaining product is washed with deionized water several times. The suspended solid was then vacuum filtered and dried at 120 °C for 20 h. The dried product is then suspended in ethanol and sonicated in order to disperse graphene sheets.

2.2. Preparation of graphene sheets-ZnO (GSs-ZnO) composite

The as-synthesized GSs (10 mg) and 0.148 g zinc acetate ($Zn(O_2CCH_3)_2$) were put in deionized water (50 ml) and stirred for 30 min at room temperature. After 30 min 0.52 ml $NH_3{*}H_2O$ solution of 0.3 M was added drop by drop. The solution was then stirred and sonicated for 10 min for homogeneous mixing. Now this solution was put into 100 ml of Teflon-lined autoclave. The autoclave was sealed and heated to 180 °C temperature for 24 h. After removing from the furnace, the material was cooled to room temperature. The black precipitated products were filtered out and washed with deionized water several times and then dried in the vacuum at 60 °C for 1 h. Synthesis of GSs and GSs-ZnO multipod nanocomposite has been carried out using autoclave reactor.

2.3. Characterization tools

The as grown carboneous materials were characterized by X-ray diffractometer (XRD, Philips PW 1710), transmission electron microscopy (TEM, Tecnai G^2 20). Sample for TEM studies were prepared by dispersing a small amount of carboneous materials into ethanol and sonication for 10 min. Drops of the dispersed material were placed onto a holey carbon grid and dried. Raman spectroscopy of the as-grown sample was carried out by Raman spectrometer (Renishaw, model no. H 45517) using an argon ion laser (λ = 514 nm). Fourier transform infrared (FTIR) spectra of the samples were recorded using the Perkin-Elmer (Spectrum 100, USA) spectrometer. The photoluminescence (PL) spectrum at room temperature was measured by a PerkinElmer LS 55 type luminescence spectrometer having Xe lamp of 350 nm line as an excitation source.

3. Results and discussion

3.1. Microstructural characterization

3.1.1. Characterization of graphene sheets (GSs)

X-ray diffraction (XRD) measurements were employed to investigate the phase and structure of the synthesized samples. Typical XRD pattern of GSs sample is shown in Fig. 1. The inset of Fig. 1 shows the (0 0 2) reflection around 24.9° (blue line) and a broad peak around 18.7° (blue line) which are merged to give the resultant peak (red line). The (0 0 2) graphitic reflection in the powder XRD pattern of sample shows that it comprises of few numbers of GSs. The number of layers in GSs samples can be obtained by Lorentzian fitting of the (0 0 2) reflection making the use of the Scherrer formula [31]. Inset of Fig. 1 shows multiple Lorentzian fitting of the (0 0 2) reflection. The number of layers in GSs has been found to be 2 and 8 correspond to the broader peaks at 18.7° and 24.9° respectively [32]. The inter layer separations between GSs are 0.41 and 0.35 nm corresponding to the peak at 2θ = 18.7° and 24.9° respectively.

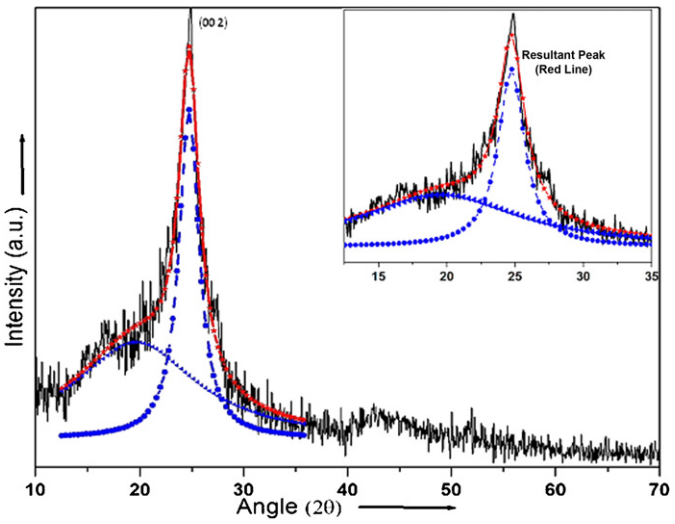

Fig. 1. XRD patterns of GSs samples. Inset shows the multiple Lorentzian fitting of the (0 0 2) reflections. (For interpretation of the references to color in the text, the reader is referred to the web version of the article.)

Fig. 2 shows the SEM micrographs of the as-synthesized graphene sample prepared by solvothermal method. The bulk GSs product obtained from the pyrolysis of the solvothermal product is highly porous as well as flaky. The entire micrograph consists of individual GSs held into a porous structure that typically extends over more than 10 μm, with the presence of numerous cavities, or holes. The GSs are therefore, initially obtained as fused sheets, weakly held into a foam-like structure which is then easily separated into individual sheets by sonication in ethanol for several minutes.

Fig. 3 presents the low resolution TEM micrographs of the agglomerated GSs at different magnification. This clearly shows the extent of sheet formation and the tendency for sheets to coalesce into overlapped regions. An inherent sheet-like structure displaying an intricate long-range array of folds is evident. TEM micrograph shows that GSs has corrugations and scrolling on the edge of the graphene (shown by arrow). The images are taken in transmission mode; the relative opacity of individual sheets is a result of interfacial regions with overlap between individual sheets [33]. The GSs are transparent and exhibit a very stable nature under the electron beam. The SAED pattern (inset in Fig. 3(b)) shows the well-defined diffraction spots, which confirm the crystalline structure of the GSs.

Fig. 4 shows the HRTEM micrograph of GSs which are clearly visible. HRTEM micrograph shows the morphology of few-layer GSs. The numbers of GSs are found to be 3, 4 and 7 layered, which are in conformity with the results of XRD analysis (Fig. 1).

3.1.2. Characterization of graphene sheets-ZnO (GSs-ZnO) multipod nanocomposite

Fig. 5 shows the diffraction peaks of as-synthesized GSs-ZnO multipod nanocomposite. The peaks at 2θ = 31.7°, 34.4°, 36.2°, 47.5°, 56.6°, 62.8°, 66.3°, 67.9°, and 69.1° correspond to the (1 0 0), (0 0 2), (1 0 1), (1 0 2), (1 1 0), (1 0 3), (2 0 0), (1 1 2) and (2 0 1)

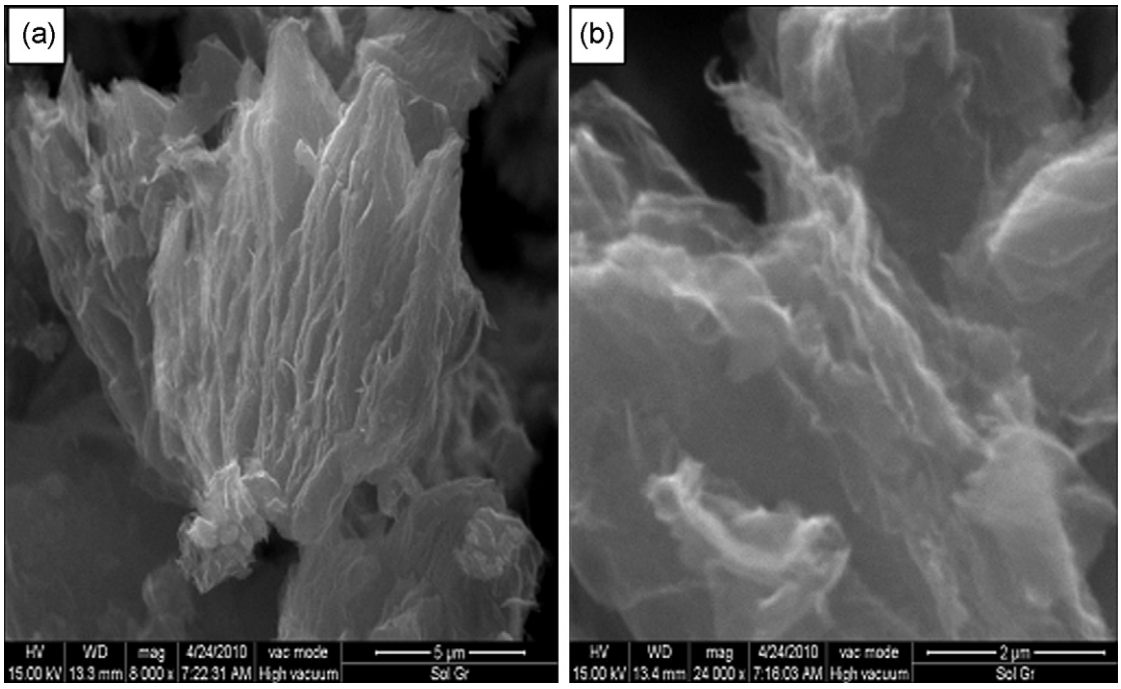

Fig. 2. SEM micrographs of as-synthesized GSs.

crystalline planes of ZnO, respectively. This result indicates that the ZnO multipod on the GSs is having wurtzite structure. The peak at 44.4 corresponds to the specimen holder used for XRD. The (0 0 2) graphitic reflection is also present in the powder XRD pattern of sample, which corresponds to GSs.

Transmission electron microscopy (TEM) and high resolution transmission electron microscopy (HRTEM) analyses were performed on the as-prepared GSs-ZnO multipod nanocomposites to determine their features in the nanometer domain. Fig. 6 shows the TEM micrographs of GSs-ZnO multipod nanocomposite synthesized by the hydrothermal method. TEM micrograph (Fig. 6) shows the intimate contact between ZnO multipod (marked by arrow) and GSs (mark by dotted arrow). This intimate contact makes the electronic interaction between ZnO multipod and GSs possible. The lengths of the legs of ZnO multipod were found to be in the range of 200–250 nm. It can be clearly seen that the GSs were well decorated by ZnO multipods, which were densely deposited on these GSs to form a composite structure. Moreover, almost no ZnO multipods were found outside the GSs. Some larger features shown in Fig. 6 are agglomerate of ZnO multipods.

The structure of GSs-ZnO multipod nanocomposite was further investigated by HRTEM. Fig. 7 shows the HRTEM of the leg of ZnO multipod which is showing (0 0 2) plane [34–36]. The interplanar spacing is found to be 0.26 nm corresponding to the (0 0 2) crystal plane.

Fig. 8 shows the typical energy dispersive X-ray of as-synthesized GSs-ZnO multipod nanocomposite. The EDX has been taken from larger area with different regions. The elemental analysis of GSs (Fig. 8(a)) shows the presence of carbon and oxygen contents. Fig. 8(b) shows the elemental content of carbon, oxygen and zinc in GSs-ZnO multipod nanocomposite sample. The presence of zinc, oxygen and carbon indicate the formation of GSs-ZnO multipod nanocomposite. There is some change in oxygen content, which shows the reduction of oxygen from GSs.

3.2. Fourier transform infrared analysis

Fourier transform infrared (FTIR) study in the range of 4000–450 cm^{-1} has been carried out in the present investigation. The FTIR spectrum of as-synthesized GSs and GSs-ZnO multipod nanocomposite are shown in Fig. 9. The peaks in Fig. 9(a) and

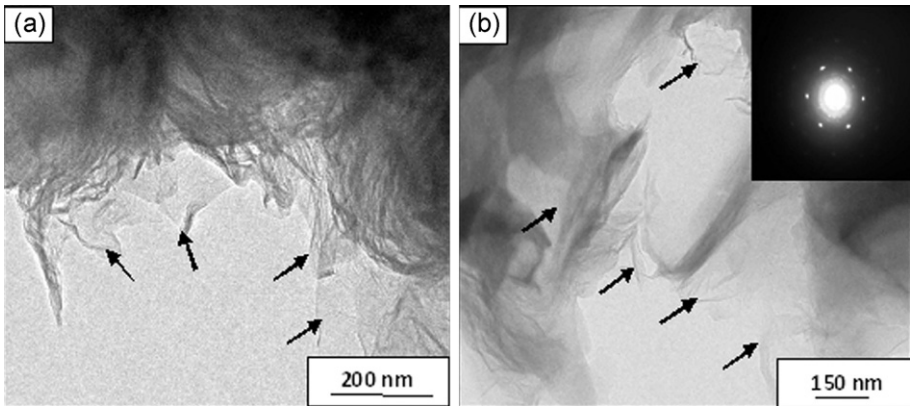

Fig. 3. TEM micrographs of the agglomerated GSs.

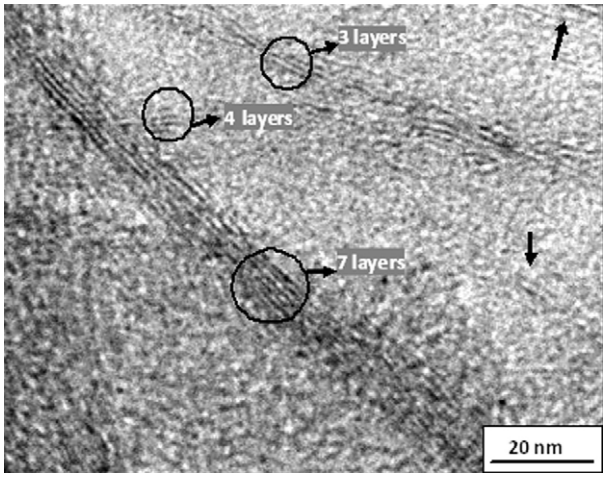

Fig. 4. HRTEM micrograph of the as synthesized GSs.

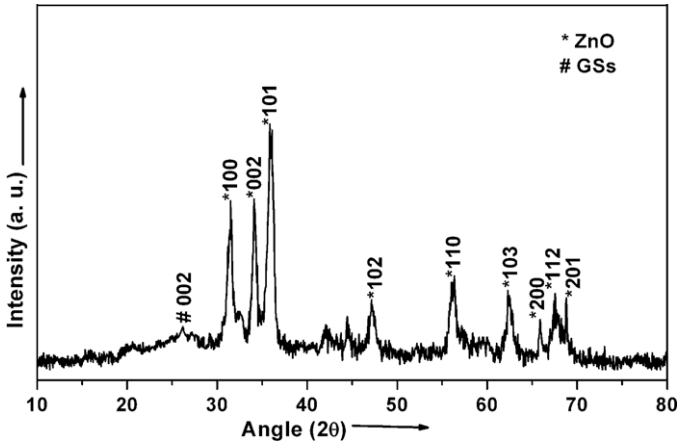

Fig. 5. XRD pattern of GSs-ZnO multipod nanocomposite sample.

(b) at 3440 cm^{-1} indicates the presence of OH groups, which are due to the presence of moisture in the samples. In GSs (Fig. 9(a)) the peak at 1636 cm^{-1} can be assigned to the vibrations of unoxidized graphitic domains [37]. The small oxygen-containing functional groups attach to GSs are revealed by the bands at 1392 cm^{-1} and 1045 cm^{-1}, which correspond to C—OH stretching

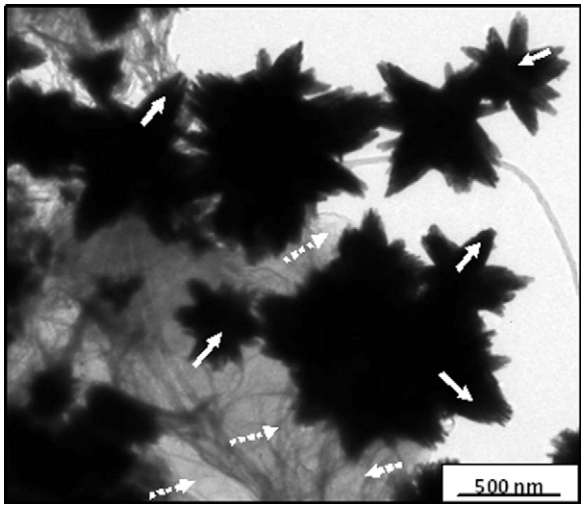

Fig. 6. TEM micrograph of as synthesized GSs-ZnO multipod nanocomposite.

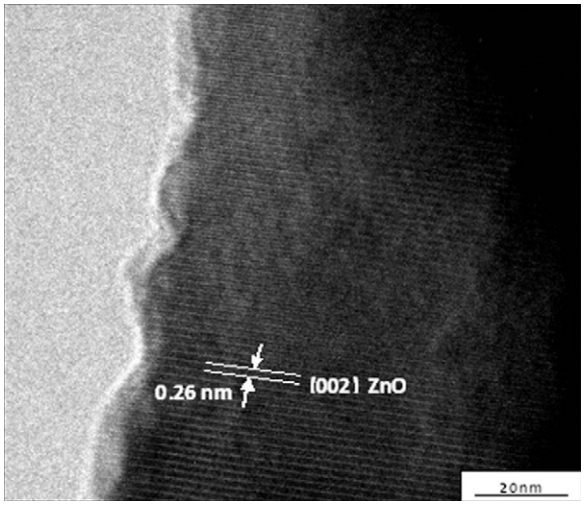

Fig. 7. HRTEM micrograph of as synthesized GSs-ZnO multipod nanocomposite.

and C—O stretching vibrations respectively [38]. In GSs-ZnO multipod nanocomposite (Fig. 9(b)), the strong peak at 1552 cm^{-1} can be attributed to the skeletal vibration of the GSs and other peak at 465 cm^{-1} is the characteristic peak of the Zn—O stretching vibration of ZnO [39,40]. There are no signature of peaks at 1392 cm^{-1} and 1045 cm^{-1} corresponding to functional groups containing oxygen in GSs-ZnO multipod nanocomposite. However, at 3400 cm^{-1} there is a broad peak of small size indicating the presence of OH

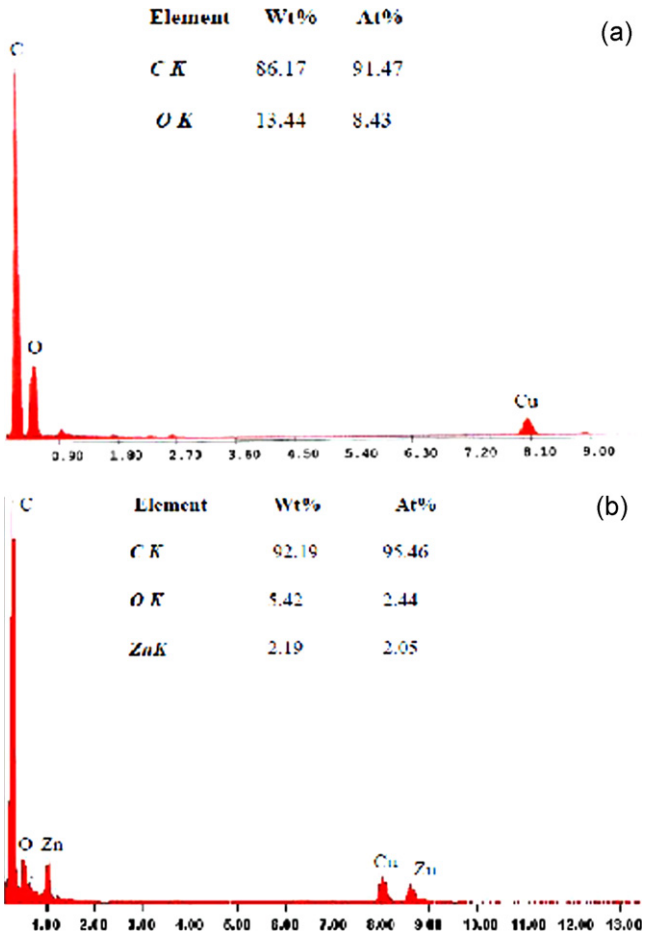

Fig. 8. Energy dispersive X-ray of: (a) as-synthesized GSs and (b) GSs-ZnO multipod nanocomposite.

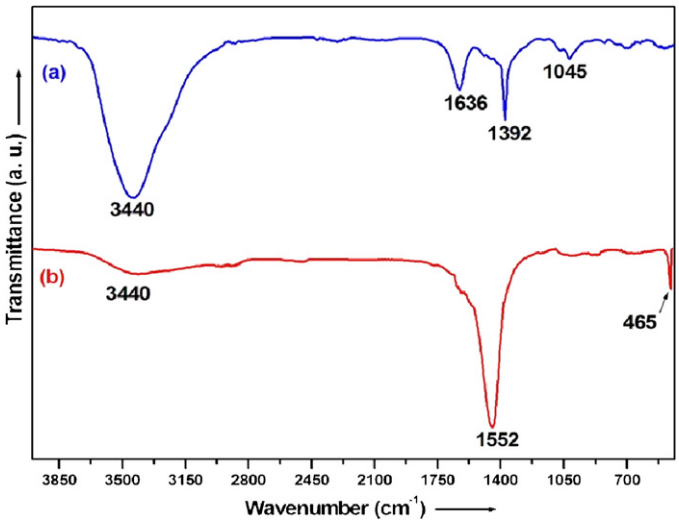

Fig. 9. FTIR of as synthesized (a) GSs and (b) GSs-ZnO multipod nanocomposite.

group. This has also been confirmed by EDX analysis in Fig. 8. These observations confirm that the GSs-ZnO multipod nanocomposite has been successfully prepared. Further it may be mentioned that from these observations, it appears that GSs are not completely devoid of oxygen containing functional groups, which are attached to these sheets. Because of these functional groups, the separation between sheets is somewhat larger than the graphitic planes and smaller than the interplanar separation between graphene oxide layers.

3.3. Raman analysis

Fig. 10(a) and (b) shows the Raman spectra of GSs and GSs-ZnO multipod nanocomposite, respectively. Both samples exhibit two peaks namely D-band and G-bands. The D-band is associated with the presence of defects in the hexagonal graphitic layers, and the G-bands is associated with Raman-active E_{2g} modes, which are usually assigned to the breathing mode of κ point phonons of A_{1g} symmetry and the E_{2g} phonon of C sp^2 atoms, respectively [41]. It may be noted that the Raman D-band peak of GSs at 1340 cm^{-1} has shifted to 1348 cm^{-1} in GSs-ZnO multipod nanocomposite, i.e. shifted towards the higher wave number. Raman G-bands peak

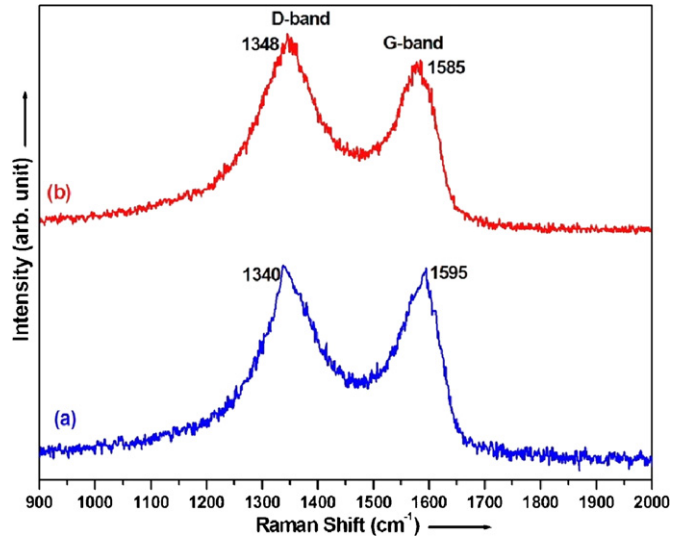

Fig. 10. Raman spectra of as-synthesized (a) GSs and (b) GSs-ZnO multipod nanocomposite.

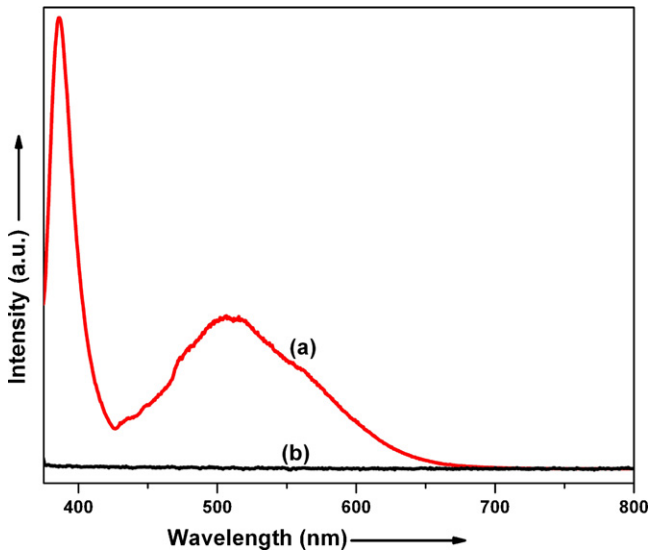

Fig. 11. Room-temperature PL spectra of (a) ZnO multipod and (b) GSs-ZnO multipod nanocomposite.

of GSs at 1595 cm^{-1} has shifted to 1585 cm^{-1} in GSs-ZnO multipod nanocomposite, i.e. is shifted towards the lower wave number. These observations show that the D band has been slightly blue-shifted by 8 cm^{-1} in the GSs-ZnO multipod nanocomposites, while the G band has shown a red shift of 10 cm^{-1}. Similar shifts for the case of graphene-ZnO nanoparticle composite have also been reported [42]. These shifts in the Raman peak have been attributed to the chemical interaction between GSs and ZnO multipod. The I_D/I_G ratio has been found to increase from 1.0 to 1.25 for GSs to GSs-ZnO multipod nanocomposite. This indicates the existence of reduction of graphene and interaction between GSs and ZnO multipod [43,44].

3.4. Photoluminescence spectrum analysis

In order to explore the potential optical and electronic applications, the PL emission spectrum of as-prepared GSs-ZnO multipod nanocomposite was measured. The excitation source employed here was the 350 nm line of Xe lamp. In the PL spectrum of pure ZnO multipod, the near band edge (NBE) emission of ZnO is seen around 380 nm (3.22 eV) (Fig. 11(a)). The near-UV emissions at 3.20 eV correspond to the bulk bandgap at 3.35 eV of ZnO and originate from the recombination of free excitons. In Fig. 11(a), a broad PL emission peak is found in the wavelength range of 400–700 nm, which is attributed to the oxygen vacancies in ZnO lattice [45]. This type of broad PL emission has also been reported for ZnO nanoparticles [46]. The emission peak can be assigned to the electron excited-recombined on the surface of ZnO multipod [45]. A change in the emission of GSs-ZnO multipod nanocomposite can be noticed in Fig. 11(b). The PL emission peak has been found to be quenched completely. It is interesting to note that phenomena like this were also observed in the graphene-ZnO composite [47,48]. There are also some reports available on CNTs-ZnO composite showing the quenching properties [11]. It has been proposed for the case of CNTs-ZnO composite that electrons can transfer from ZnO to the outermost surface of CNTs which act as electron acceptors [11,19]. Because of the similarity of graphene structure with CNTs, it is proposed that PL emission peak of ZnO multipod get suppressed due to the similar energy transfer mechanism.

It is known that ZnO is a good electron donor and carbon materials are relatively good electron acceptor, thus the synergistic effect between these two components would effectively reduce recombination and lead to an increased charge carrier separation [38].

Luminescence quenching of the emission of ZnO in the visible region was observed in such coupling systems, which also provide a facile method to monitor the interfacial electron-transfer processes [42,49]. Charge recombination in semiconductor particulates is often a problem in solar cells based on mesoscopic semiconductor films. If semiconductor particles are anchored on a graphene scaffold, it should be possible to improve the photo induced charge separation. The PL results imply that the graphene-ZnO composites have potential application in the photo-electrochemical cell [18].

Based on our experimental results, formation of GSs-ZnO multipod nanocomposite can be understood in terms of electrostatic interaction mechanism. The small amount of oxygen-containing groups in GSs is negatively charged due to the functional groups attached to the GSs surfaces [43,44]. When zinc acetate is mixed with GSs, the positive Zn^{2+} may get absorbed on the surface of GSs due to electrostatic interaction. These Zn ions will react with $NH_3{}^*H_2O$ on the GSs surface to form ZnO clusters. Although the exact mechanism of multipod formation is not known at present, some plausible explanation may be given. The initial shape of ZnO nucleus will be governed by the growth conditions, e.g. temperature, concentration of Zn^{2+} and $NH_3{}^*H_2O$, etc. Since the c-direction of ZnO is the fastest growth direction; the legs of multipods have grown along this direction. It is also evident from HRTEM image (Fig. 7). Probably, the multipods are growing on the clusters of ZnO particles having (0 0 0 1) surface. These ZnO multipods are spread over the surface of GSs.

In order to investigate the influence of different reaction temperatures and durations on the structural features of the final products, we have carried out comparative experiments and found out that reaction temperature and reaction time strongly affect the yield of GSs-ZnO multipod nanocomposite. In the present work, a reaction time of 24 h appears to give the largest quantity of the GSs-ZnO multipod nanocomposites than other reaction time used. Meanwhile, it has been found that the optimal reaction temperature is 180 °C, and no ZnO multipod was produced when the temperature is lower than 180 °C.

4. Conclusions

In the present work, GSs and GSs-ZnO multipod nanocomposite have been synthesized using solvothermal and hydrothermal methods, respectively. It was found that the annealing at 180 °C for 24 h in the reaction medium was crucial for the formation of GSs-ZnO multipod nanocomposite. XRD analysis and HRTEM show the presence of 2–8 layered graphene sheets. Raman and FTIR spectra clearly indicate the formation of GSs-ZnO multipod nanocomposite. The photoluminescence spectra of GSs-ZnO multipod nanocomposites exhibit a significant change with respect to ZnO multipod in the wavelength of 400–700 nm. The PL emission peak has been quenched completely for GSs-ZnO multipod nanocomposite. It would be intriguing to explore whether this fluorescence quenching property is a characteristic feature of all types of graphene sheets-ZnO (GSs-ZnO) nanocomposites.

Acknowledgements

The authors are grateful to Prof. C.N.R. Rao, Prof. A.K. Raychaudhary and Prof. A.K. Sood their encouragement and support. The Financial support from the DST, UGC, DRDO and MNRE-New Delhi, India is gratefully acknowledged. One of the authors, Rajesh Kumar is grateful to the Council of Scientific and Industrial Research (CSIR)-New Delhi, Government of India for providing a senior research fellowship.

References

[1] K.S. Novoselov, A.K. Geim, S.V. Morozov, D. Jiang, Y. Zhang, S.V. Dubonos, I.V. Grigorieva, A.A. Firsov, Science 306 (2004) 666–669.
[2] A.K. Geim, K.S. Novoselov, Nat. Mater. 6 (2007) 183–191.
[3] F. Bonaccorso, Z. Sun, T. Hasan, A.C. Ferrari, Nat. Photon. 4 (2010) 611–622.
[4] K.S. Novoselov, A.K. Geim, S.V. Morozov, D. Jiang, M.I. Katsnelson, I.V. Grigorieva, S.V. Dubonos, A.A. Firsov, Nature 438 (2005) 197–200.
[5] M.I. Katsnelson, Mater. Today 10 (2007) 20–27.
[6] J.S. Wu, W. Pisula, K. Mullen, Chem. Rev. 107 (2007) 718–747.
[7] D. Li, R.B. Kaner, Science 320 (2008) 1170–1171.
[8] H.L. Guo, X.F. Wang, Q.Y. Qian, F.B. Wang, X.H. Xia, ACS Nano. 3 (2009) 2653–2659.
[9] P. Solís-Fernández, R. Rozada, J.I. Paredes, S. Villar-Rodil, M.J. Fernández-Merino, L. Guardia, A. Martínez-Alonso, J.M.D. Tascón, J. Alloys Compd. http://dx.doi.org/10.1016/j.jallcom.2012.01.102.
[10] H.C. Schniepp, J.L. Li, M.J. McAllister, H. Sai, Herrera M. Alonso, D.H. Adamson, R.K. Prud'homme, R. Car, D.A. Saville, I.A. Aksay, J. Phys. Chem. B 110 (2006) 8535–8539.
[11] Y. Zhang, H. Li, L. Pan, T. Lu, Z. Sun, J. Electroanal. Chem. 634 (2009) 68–71.
[12] K.S. Kim, Y. Zhao, H. Jang, S.Y. Lee, J.M. Kim, K.S. Kim, J.H. Ahn, P. Kim, J.Y. Choi, B.H. Hong, Nature 457 (2009) 706–710.
[13] S. Niyogi, E. Bekyarova, M.E. Itkis, J.L. McWilliams, M.A. Hamon, R.C. Haddon, J. Am. Chem. Soc. 128 (2006) 7720–7721.
[14] K.A. Worsley, P. Ramesh, S.K. Mandal, S. Niyogi, M.E. Itkis, R.C. Haddon, Chem. Phys. Lett. 445 (2007) 51–56.
[15] J.I. Paredes, S. Villar-Rodil, P. Solís-Fernández, M.J. Fernández-Merino, L. Guardia, A. Martínez-Alonso, J.M.D. Tascón, J. Alloys Compd. http://dx.doi.org/10.1016/j.jallcom.2011.10.025.
[16] A. Rochefort, J.D. Wuest, Langmuir 25 (2009) 210–215.
[17] P. Zeng, Q. Zhang, X. Zhang, T. Peng, J. Alloys Compd. 516 (2012) 85–90.
[18] B. Seger, P.V. Kamat, J. Phys. Chem. C 113 (2009) 7990–7995;
T. Lu, L. Pan, H. Li, G. Zhu, T. Lv, X. Liu, Z. Sun, T. Chen, D.H.C. Chua, J. Alloys Compd. 509 (2011) 5488–5492.
[19] F. Vietmeyer, B. Seger, P.V. Kamat, Adv. Mater. 19 (2007) 2935–2940.
[20] A. Kongkanand, P.V. Kamat, J. Phys. Chem. C 111 (2007) 9012–9015.
[21] A. Kongkanand, R.M. Domınguez, P.V. Kamat, Nano Lett. 7 (2006) 676–680.
[22] J. Wang, Z. Gao, Z. Li, B. Wang, Y. Yan, Q. Liu, T. Mann, M. Zhang, Z. Jiang, J. Solid State Chem. 184 (2011) 1421–1427.
[23] J.M. Lee, Y.B. Pyun, J. Yi, J.W. Choung, W.I. Park, J. Phys. Chem. C 113 (2009) 19134–19138.
[24] X. Liu, L. Pan, T. Lv, T. Lu, G. Zhu, Z. Sun, C. Sun, Catal. Sci. Technol. 1 (2011) 1189–1193.
[25] B. Li, H. Cao, J. Mater. Chem. 21 (2011) 3346–3349.
[26] Y. Chen, X. Zhang, D. Zhang, Y. Ma, J. Alloys Compd. 511 (2012) 251–256.
[27] C. Jagdish, S. Pearton, Elsevier Oxford IX51GB, UK, 2006.
[28] J. Singh, S.S. Patil, M.A. More, D.S. Joag, R.S. Tiwari, O.N. Srivastava, Appl. Surf. Sci. 256 (2010) 6157–6163.
[29] J. Singh, R.S. Tiwari, O.N. Srivastava, J. Nanosci. Nanotechnol. 7 (2007) 1783–1786.
[30] M. Choucair, P. Thordarson, J.A. Stride, Nat. Nanotech. 4 (2009) 30–33.
[31] A.W. Burton, K. Ong, T. Rea, I.Y. Chan, Micropor. Mesopor. Mater. 117 (2009) 75–90.
[32] C.N.R. Rao, K. Biswas, K.S. Subrahmanyam, A. Govindaraj, J. Mater. Chem. 19 (2009) 2457–2469.
[33] J.C. Meyer, A.K. Geim, M.I. Katsnelson, K.S. Novoselov, T.J. Booth, S. Roth, Nature 446 (2007) 60–63.
[34] Y. Tian, H.B. Lu, L. Liao, J.C. Li, C. Liu, Solid State Commun. 149 (2009) 456–460.
[35] L. Jiang, L. Gao, Mater. Chem. Phys. 91 (2005) 313–316.
[36] J.M. Feng, Y.L. Li, F. Hou, X.H. Zhong, Mater. Sci. Engg. A 473 (2008) 238–243.
[37] H.K. Jeong, Y.P. Lee, R.J. Lahaye, M.H. Park, K.H. An, I.J. Kim, C.W. Yang, C.Y. Park, R.S. Ruoff, Y.H. Lee, J. Am. Chem. Soc. 130 (2008) 1362–1366.
[38] J.L. Wu, X.P. Shen, L. Jiang, K. Wang, K.M. Chen, Appl. Surf. Sci. 256 (2010) 2826–2830.
[39] C. Nethravathi, M. Rajamathi, Carbon 46 (2008) 1994–1998.
[40] N. Lepot, M.K.V. Bael, H. Rul, D.H.J. Vanden, R. Peeters, D. Franco, Mater. Lett. 61 (2007) 2624–2627.
[41] A.C. Ferrari, J.C. Meyer, V. Scardaci, C. Casiraghi, M. Lazzeri, F. Mauri, S. Piscanec, D. Jiang, K.S. Novoselov, S. Roth, A.K. Geim, Phys. Rev. Lett. 97 (2006) 187401–187404.
[42] T.G. Xu, L.W. Zhang, H.Y. Cheng, Y.F. Zhu, Appl. Catal. B: Environ. 101 (2011) 382–387.
[43] S. Stankovich, D.A. Dikin, R.D. Piner, K.A. Kohlhaas, A. Kleinhammes, Y. Jia, Y. Wu, S.T. Nguyen, R.S. Ruoff, Carbon 45 (2007) 1558–1565.
[44] S. Park, J. An, I. Jung, R.D. Piner, S.J. An, X. Li, A. Velamakanni, R.S. Ruoff, Nano Lett. 9 (2009) 1593–1597.
[45] Z.Y. Jiang, Z.X. Xie, X.H. Zhang, S.C. Lin, T. Xu, S.Y. Xie, R.B. Huang, L.S. Zheng, Adv. Mater. 16 (2004) 904–907.
[46] J. Liu, X. Li, L. Dai, Adv. Mater. 18 (2006) 1740–1744.
[47] W. Zou, J. Zhu, Y. Sun, X. Wang, Mater. Chem. Phys. 125 (2011) 617–620.
[48] Y. Yang, T. Liu, Appl. Surf. Sci. 257 (2011) 8950–8954.
[49] O. Akhavan, Carbon 49 (2010) 11–18.